Design of a 3D Intelligent Building Management Framework that Integrates Geographic Information Systems and Building Information Models

Dong Zheng[1], Hairong Huang[2*], Rongxing Wu[3]
[1]Ningbo Polytechnic, Ningbo, 315800, China
[2]School of Architecture and Engineering, Zhejiang Tongji Vocational College of Science and Technology, Hangzhou, 311200, China
[3]School of Architecture and Art, Ningbo Polytechnic, Ningbo, 315800, China
[*]E-mail: 13355991013@163.com
[*]Corresponding author

Keywords: geographic information systems, building information model, 3D, oblique photography

Recieved: April 14, 2024

Promoting the construction of 3D intelligent buildings is one of the important paths to achieve high-quality development in the new stage of architecture. This study first constructs a 3D model of an intelligent building based on a building information model, and then collects environmental data using the constructed geographic information system. Finally, a semantic constraint-based transformation approach is employed to integrate multi-source data, including geographic information system data and building information model data to construct a 3D intelligent building management framework system. The results showed that the selected optimization algorithm could effectively compress the data of the 3D model. Taking the "Car" 3D model data as an example, it could be compressed to 66.4% of the original file. Moreover, in the simplification process, the research method had better results in detail processing. The constructed system could quickly complete the rendering of the 3D model at different distances. The rendering time of the system for the overall appearance of intelligent buildings, intelligent system equipment, and 3D models of pipelines was 9.1s, 12.0s, and 7.2s, respectively. The frame rates during rendering were 35.2-46.2FPS, 27.6-38.1FPS, and 48.2-53.1FPS, respectively. This system achieves precise modeling and management of intelligent buildings, providing theoretical support for the construction of similar building management systems.

Povzetek: Razvit je 3D programski okvir (platforma) za upravljanje inteligentnih stavb, ki integrira GIS in BIM podatke z uporabo semantičnih omejitev. Razvita metoda omogoča učinkovito obdelavo, zmanjšanje podatkov in hitro izrisovanje 3D modelov, kar prispeva k natančnemu modeliranju in učinkovitemu upravljanju inteligentnih stavb.

1 Introduction

The acceleration of urbanization has made the design and management of buildings increasingly complex. Traditional architectural design and management mainly rely on draft design and manual statistics, which are time-consuming, labor-intensive, and prone to errors. Moreover, these methods are difficult to conduct detailed data analysis and management [1-2]. With the continuous maturity of Building Information Model (BIM) and Geographic Information System (GIS) technologies, their applications in building design and management have become increasingly widespread [3]. The BIM has a high degree of refinement, but it cannot be combined with the surrounding geographic information environment [4]. GIS can precisely analyze geographic space, combining the advantages of the two, and can achieve rapid application of Intelligent Building Management (IBM) design. However, the data information of these two cannot be directly integrated, and BIM has the problem of large data volume, while GIS has the problem of incomplete geographic data collection [5]. Based on this background, this study adopts semantic constraint-based transformation to integrate the multivariate data of GIS and BIM. This integration is intended to address the existing limitations of GIS and BIM, and to construct a 3D IBM framework system. It is expected to achieve precise construction and efficient management of 3D intelligent buildings. The research content consists of four chapters. Chapter 1 mainly explains the current development status of intelligent buildings and the latest achievements in the integration of GIS and BIM applications. Chapter 2 first explains the construction of BIM and data lightweight processing, then explains the geographic environment information collection and processing methods of GIS models, and finally constructs a 3D IBM framework system. Chapter 3 mainly designs experiments to analyze the performance of the selected method and the application effect of building a 3D model of the system.

Chapter 4 mainly analyzes the experimental results and elaborates on the shortcomings of the research as well as future research directions.

2 Related works

In the 1970s, developed countries began to rise in green intelligent buildings, introducing the concept of intelligent buildings, which has attracted extensive research from many experts and scholars. Yu et al. discussed the importance and urgency of developing Intelligent Building Energy Management (IBEM) technology, and suggested that IBEM should develop accurate and efficient building thermodynamic models while addressing operational constraints coupled in space and time [6]. Edirisinghe and Woo proposed the real-time capture and visualization of building performance data using wireless sensor network measurement data and user perception data based on mobile applications to manage intelligent building facilities. Innovative data capture and visualization technologies have been effectively applied in the practice of intelligent building facilities [7]. Pan and Zhang artificially enhanced IBM's capabilities by integrating BIM and artificial intelligence (AI), creating a management framework that includes automated design and rule checking, 3D scene reconstruction, event log mining, building performance analysis, virtual and augmented reality, and digital twins. Integrating BIM and AI had potential value and practical utility throughout the entire lifecycle of intelligent building projects [8]. However, these solutions for intelligent building design and management are still far from meeting people's needs.

In recent years, BIM has been widely recognized as a core technology in the construction industry. It is based on traditional construction techniques and integrates information from various stages of construction project planning to operation into a complete model, effectively improving the efficiency of the project. However, BIM technology has limitations in spatial analysis, while GIS can compensate for the shortcomings of BIM technology by analyzing the geographic spatial data of the surrounding environment. Therefore, the development of smart cities will depend on the combination of BIM and GIS technology. Many experts and scholars have also conducted in-depth research on the integration of BIM and GIS technologies. Abd et al. proposed using robots for construction work to address the issue of low productivity in the construction industry, and utilizing BIM and GIS technologies to provide a comprehensive digital building environment that robots may utilize. However, this study only analyzed the requirements of BIM-GIS integration for robot positioning from a theoretical perspective [9]. Asgari Siahboomy et al. discussed the latest progress of BIM and GIS in manufacturing and project management, and pointed out that the integration of BIM and GIS can bring multiple advantages for optimizing warehouse positioning in large manufacturing factories. Meanwhile, its use of BIM tools to simulate and locate the product warehouse in EMSC's casting workshop confirmed the feasibility of this method [10]. Zhu et al. proposed a solution and developed an algorithm to interpret scanned entity profiles in IFC to address the data conversion issue between Industry Foundation Classes and shape files when integrating BIM and GIS. Finally, the possible uses of the transformed shape file model were demonstrated through a bridge management system based on Web GIS [11]. AlSaggaf and Jrade proposed a multi-functional and flexible site layout planning model to address the issue of differences between BIM and GIS when developing and integrating them for site layout planning. This model could effectively address the differences in the model [12]. Dinis et al. found in their research on the development of semantic enhancement systems and applications in BIM that there are constraints on sharing semantic data between BIM and GIS platforms, and solving this problem required a broader transformation of BIM paradigms [13].

According to the above information, intelligent buildings will be the development direction of future buildings, and the integration of BIM and GIS technology is an inevitable trend to achieve rapid development of intelligent buildings. At present, although BIM and GIS technologies have made significant progress in their respective fields, their integration is still in its early stages and is not yet mature, and there are still many technical deficiencies. In view of this, this study focuses on 3D intelligent buildings, using BIM to provide building information, GIS for information collection and visualization display, and connecting the information data of the two through format conversion. Therefore, the goal is to achieve the organic integration of building models and spatial environmental information data, and to build an IBM framework that can accurately model and efficiently manage. The summary of relevant work is shown in Table 1.

Table 1: Summary of related work

Author(s)	Year	Methodology	Key Findings	Limitations
Abd et al. [9]	2020	Propose the use of robots for construction work and utilize BIM and GIS technologies to provide a comprehensive digital building environment that robots may utilize.	\	Only at the theoretical level
Asgari	2021	Discussed the latest progress of BIM	The integration solution of	The integration of

Siahboomy et al. [10]		and GIS in manufacturing and project management	BIM and GIS can provide system simulation for optimizing warehouse positioning in large manufacturing factories	BIM and GIS data poses certain difficulties
Zhu et al. [11]	2021	Developed algorithms to interpret scanned entity profiles in IFC, and demonstrated the possible uses of the transformed shape file model through a Web GIS based bridge management system	Solved the data conversion issue between Industry Foundation Classes and shape files	The efficiency of the system is not high
AlSaggaf et al. [12]	2023	Proposed a multifunctional and flexible site layout planning model	Integrating BIM and GIS data differences	The model is relatively complex
Research method	2024	A method of data transformation based on semantic constraints	The model integrates the differences between BIM and GIS data, and has a simple structure and high efficiency.	The system management module has a relatively single function

3 Design of 3D IBM framework based on GIS and BIM

Firstly, the Autodesk BIM platform is employed to construct a BIM and to simplify the 3D model data by means of an edge folding algorithm based on quadratic error measurement. Then, a GIS model is built using the SuperMap series software, and the data images are optimized using Beam Method Regional Network Adjustment (BMRNA) and Fabric Simulation Filtering (FSF) algorithms. Finally, the data information from BIM and GIS models is fused from multiple sources to construct a 3D IBM framework system.

3.1 Construction of 3D intelligent building BIM model

BIM technology is employed in the construction of intelligent buildings. This is achieved through the use of 3D digital simulation technology, which enables the construction of buildings based on specific information derived from project engineering. The technology also facilitates engineering decision-making and management by simulating real situations. This study uses the mainstream Autodesk BIM platform to build a BIM. This platform is mainly centered around Revit and provides model design solutions for intelligent building information, as shown in Figure 1.

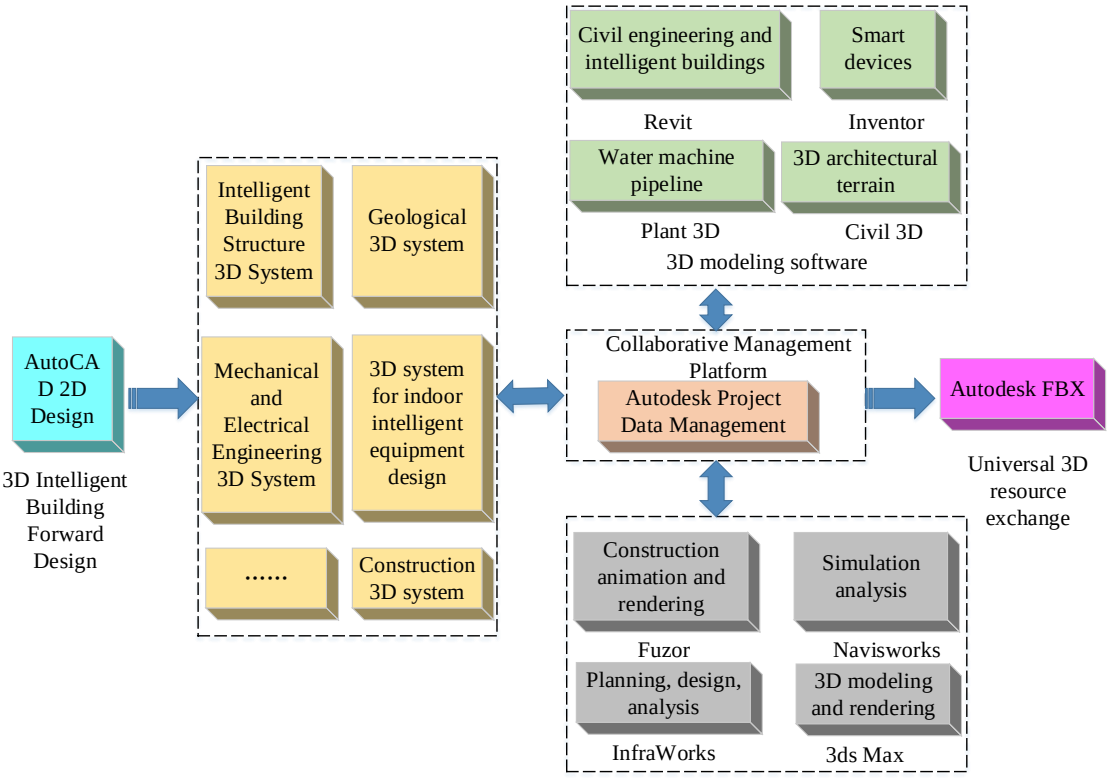

Figure 1: Process of managing 3D smart buildings on the Autodesk BIM platform

Figure 1 illustrates the utilization of Autodesk Project Data Managers as a collaborative management platform. This platform integrates information data, including intelligent building models, drawings, and project materials. It also facilitates the orderly connection of each module's functions through the setting of permissions, task allocation, and document management. The main functional modules include the following points. InfraWorks is used for project planning and design, while Revit is used for rapid modeling of various disciplines. Dynamo plugins improve modeling efficiency, while Inventor is used for intelligent device modeling. Civil3D is used for geological modeling and infrastructure design, Navisworks is used for model collision detection and construction simulation, and Fuzor is used for construction animation production and VR roaming. The Revit software of Autodesk BIM is adopted to construct 3D refined models of 3D smart buildings and assign corresponding attribute information to each 3D model. The modeling steps are shown in Figure 2.

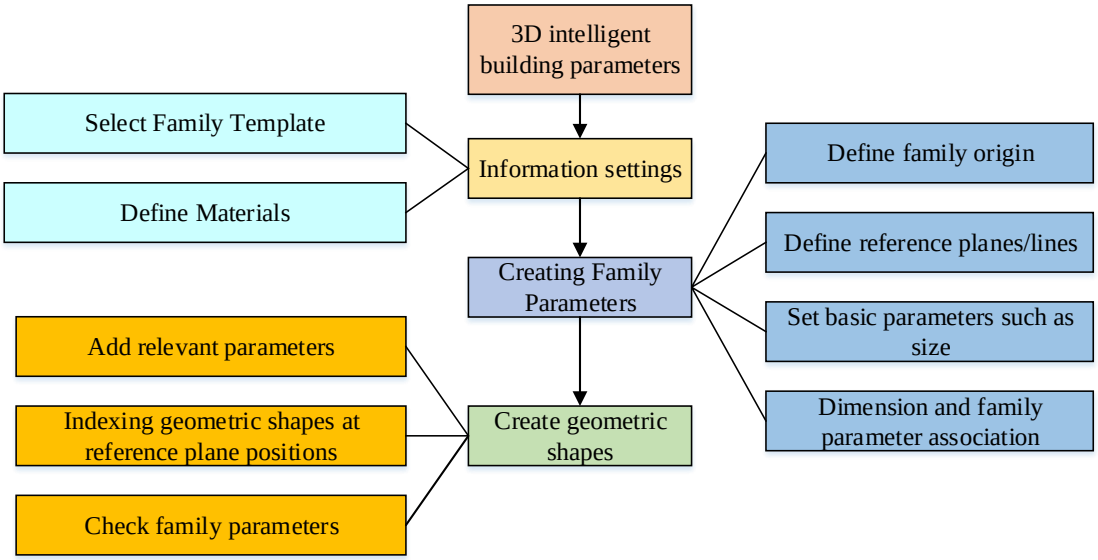

Figure 2: Specific steps for parameterized modeling

In Figure 2, the first is to design the basic outline and structural parameters of the intelligent building, and use Revit software to draw basic graphics such as squares, cylinders, and triangles to build the main body of the 3D intelligent building. Then, the internal information of the intelligent building body is added, its height, length, diameter, and name are set. Next, intelligent devices for smart buildings are designed, including intelligent lighting systems, intelligent constant temperature systems, intelligent safety systems, energy management systems, smart home systems, etc. The design method is consistent with the main body construction method, and then technical parameters, input functional rate, cooling capacity, heating capacity, etc. are added. For the design of pipelines, based on the requirements and samples of intelligent buildings, the position of the pipeline is determined through cylindrical shapes, and the accurate labeling of the pipeline diameter, installation of connecting components. Flow rate and diameter parameter settings are ensured, ultimately confirming the correct association between the pipeline and other components. Due to the large volume of BIM twin data in the constructed 3D intelligent building, lightweight processing is required. This study uses the Quadric Error Metrics (QEM) grid simplification algorithm based on quadratic error measurement to simplify the data. The main objective of quadratic error measurement is to reduce the number of vertices and faces while maintaining the geometric characteristics of the mesh.

The triangles surrounding the vertices in the original model are defined as a set of planes. After folding one of the edges, a new vertex will appear. The sum of squared distances from the new vertex to the original set of planes is the error value, as shown in equation (1).

$$\Delta(v)=\Delta\left(\left[v_x v_y v_z\right]^T\right)=\sum\left(p^T v\right)^2 \tag{1}$$

In equation (1), $\Delta(v)$ is the error measure compared to the original triangle vertex. v_x, v_y and v_y represent the x, y, and z vertices of the model's triangular mesh, respectively. p is a defined set of planes. For the convenience of calculation, the error measurement is rewritten as shown in equation (2).

$$\Delta(v)=\sum\left(p^T v\right)^2=\sum\left(p^T v\right)\left(p^T v\right)=\sum v^T\left(pp^T\right)v=vT\left(\sum K_p\right)v \tag{2}$$

In equation (2), K_p is the sum of squared

distances from any vertex in the plane to plane p. The calculation method is equation (3).

$$K_p = \begin{bmatrix} a^2 & ab & ac & ad \\ ab & b^2 & bc & bd \\ ac & bc & c^2 & cd \\ ad & bd & cd & d^2 \end{bmatrix} \tag{3}$$

The obtained quadratic curves are added and the Q matrix is defined to represent the entire plane set. The quadratic error matrix is used to represent vertices, as shown in equation (4).

$$Q_{(v_i)} = \sum_{p \in planes(v_i)} K_p \tag{4}$$

In equation (4), $planes(v_i)$ is the set of triangular faces containing v_i. If the vertices v_1 and v_2 of a certain edge of the model's triangular mesh collapse to a new vertex v_{new}, then the cost matrix of the new vertex is equation (5).

$$Q_{new} = Q_1 + Q_2 \tag{5}$$

To ensure minimal grid changes during lightweight processing, it is necessary to find the optimal v_{new}. Firstly, the Q matrix of the initial vertices is calculated, and then valid pairs are selected from it. Next, for each effective pair of (v_1, v_2), the algorithm calculates the optimal contraction target vertex v_{new}. The error generated by shrinking this pair of vertices is the cost of shrinking this pair of vertices. Subsequently, the algorithm puts all "cost pairs" into a "heap" and ensures that the "pair" with the lowest cost is located at the top of the "heap". Finally, during the iteration process, the algorithm continuously removes the least expensive pair (v_1, v_2) from the heap, performs a contraction operation, and updates the cost of all "effective pairs" involving vertex v_1 [14]. The above QEM algorithm only considers the measurement of distance. Therefore, to further improve optimization efficiency and effectiveness, the average area and vertex curvature of the triangular mesh model are introduced as constraint factors in the original model for optimization. The average area of a triangular mesh model is defined as $\bar{S}_{v0}$, as shown in equation (6).

$$\bar{S}_{v0} = \frac{\sum_{i=1}^{n} S_i}{n} \tag{6}$$

In equation (6), n represents the number of adjacent triangles. S_i is the area of the adjacent i-th triangle. For areas with rich details, introducing average area can reduce the priority of edge folding to maintain more detailed information. For flat areas, the priority of edge folding is increased to more effectively simplify the model [15]. The area of the triangle is equation (7).

$$S = \sqrt{q(q-a)(q-b)(q-b)} \tag{7}$$

In equation (7), q is 1/2 of the circumference of the triangle. a, b and c are the side lengths of the triangle, respectively. The calculation of vertex curvature is equation (8).

$$n_i = \frac{(v_i - v_{i-1})(v_{i+1} - v_i)}{\left\|(v_i - v_{i-1})(v_{i+1} - v_i)\right\|} \tag{8}$$

In equation (8), n_i is the unit vector, and v_i, v_{i-1}, and v_{i+1} are divided into three vertices. The normal vector of v_i is equation (9).

$$n_{vi} = \frac{\sum_{i=1}^{k} S_i n_i}{\left\|\sum_{i=1}^{k} S_i n_i\right\|} \tag{9}$$

The curvature C_{vi} of v_i is equation (10).

$$C_{vi} = \frac{\sum_{k} \alpha(n_{vi}, n_i)}{k} \tag{10}$$

In equation (10), k is the number of adjacent points to the vertex. $\alpha(n_{vi}, n_i)$ is the angle between the vertex normal vector and the vertex. The specific process of lightweight 3D model data using the optimized QEM algorithm is summarized in Figure 3.

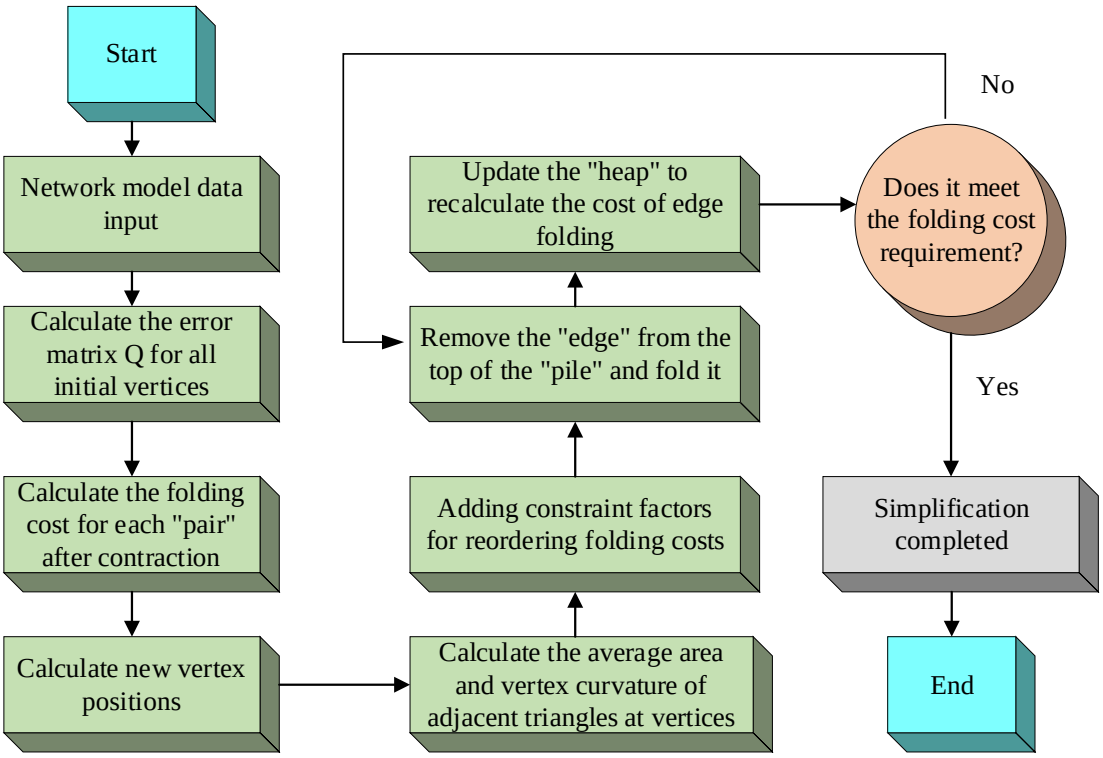

Figure 3: Simplified process steps for optimizing the Quadratic Error Measurement (QEM) algorithm

As shown in Figure 3, the first is to input the 3D model data, and use the input data to calculate the initial vertex error Q. Then, the folding cost of each pair after contraction is calculated and used to calculate the new fixed-point position. Next, the average area and vertex curve of adjacent triangles at a fixed point are calculated. Then, sorting is performed using the folding cost of constraint factors, and edges are removed from the top of the heap for folding. Finally, the "heap" is updated, the cost of folding adjacent edges is recalculated, and the previous steps are repeated until the folding meets the requirements.

3.2 GIS 3D modeling based on oblique photography

The construction of the GIS platform adopts the SuperMap series software launched by Beijing Chaotu. This software can achieve the integration of 2D and 3D model data, and can integrate multiple data sources while retaining attribute information, achieving spatial data fusion of different data formats and resolutions. The 3D geographic information data of 3D intelligent buildings mainly comes from oblique photography data. This study uses the Autel Robotics EVO series drone equipped with a 1 inch 20-megapixel OmniVision OV sensor for image data acquisition. High-definition images of the terrain, terrain, infrastructure, and other factors surrounding smart buildings are collected. After data collection, the Context Capture software based on the Bentley platform is used to reconstruct the image in 3D and construct a 3D model of the intelligent building. During 3D reconstruction, this study uses BMRNA from aerial triangulation, as shown in Figure 4.

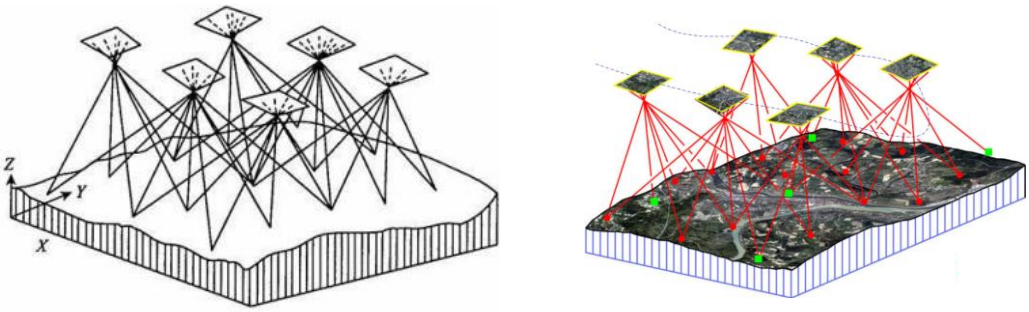

(a) Simulation diagram of beam method regional network adjustment

(b) Realistic map of beam method regional network adjustment

Figure 4: Schematic diagram of BMRNA

As shown in Figure 4, this method uses a beam of light from a single film to establish an adjustment unit, and uses the pixel coordinates as observation values for adjustment processing. By using collinear equations to rotate and translate each beam of light to achieve optimal intersection, the target area is integrated into the established control point coordinate system. According to the approximate coordinates obtained from the image, the collinear equation is listed in equation

$$\begin{cases} x = -f\dfrac{a_1(X-X_s)+b_1(Y-Y_s)+c_1(Z-Z_s)}{a_3(X-X_s)+b_3(Y-Y_s)+c_3(Z-Z_s)} \\ y = -f\dfrac{a_2(X-X_s)+b_2(Y-Y_s)+c_2(Z-Z_s)}{a_3(X-X_s)+b_3(Y-Y_s)+c_3(Z-Z_s)} \end{cases} \tag{11}$$

In equation (11), (x, y) is the coordinate of the pixel. (X, Y, Z) is the coordinate of the object point. (X_s, Y_s, Z_s) is the coordinate of the projection center. (a_i, b_i, c_i) is the coefficient. For the convenience of adjustment calculation, it is expanded into a linear form using the Taylor formula, as shown in equation (12).

$$V = \begin{bmatrix} A & B \end{bmatrix} \begin{bmatrix} t \\ X \end{bmatrix} - L \tag{12}$$

In equation (12), A, B is the corresponding coefficient matrix. t is the correction number for the external orientation elements of the image. X is the correction number for the point coordinates. The specific calculation method is equation (13).

$$\begin{cases} t = \begin{bmatrix} dX_s & dY_s & dZ_s & d\varphi & d\omega & d\kappa \end{bmatrix}^T \\ X = \begin{bmatrix} dX & dY & dZ \end{bmatrix} \\ A = \begin{bmatrix} a_{11} & a_{12} & a_{13} & a_{14} & a_{15} & a_{16} \\ a_{21} & a_{22} & a_{23} & a_{24} & a_{25} & a_{26} \end{bmatrix} \\ B = \begin{bmatrix} -a_{11} & -a_{12} & -a_{13} \\ -a_{21} & -a_{22} & -a_{23} \end{bmatrix} \\ L = \begin{bmatrix} l_x \\ l_y \end{bmatrix} \end{cases} \tag{13}$$

The corresponding normal equation can be found in equation (14).

$$\begin{bmatrix} A^T A & A^T B \\ B^T A & B^T B \end{bmatrix} \begin{bmatrix} t \\ X \end{bmatrix} = \begin{bmatrix} A^T L \\ B^T L \end{bmatrix} \tag{14}$$

By iterating multiple times, the coordinates of the encrypted points can be calculated, and external directional element information such as the pose of the image and the coordinate difference of the camera station can be obtained. Inconsistent viewpoints or small overlapping ranges between multiple images may result in a lack of points with the same name, and similar image textures may lead to multiple duplicate points with the same name. Therefore, this study adopts the method of dense matching of multi-view image area networks to correct incorrect matching coordinates in images, thereby obtaining the coordinate points of multi-view images more accurately and efficiently. The algorithm with high efficiency and low error is the FSF algorithm. When FSF processes point cloud data, the position and shape of the fabric at a specific time are determined by the force acting on the particles, and the relationship between the particle position and its force is equation (15) [16].

$$m\frac{\partial X(t)}{\partial t^2} = F_{ext}(X,t) + F_{\text{int}}(X,t) \tag{15}$$

In equation (15), X represents the position of the particle at time t. $F_{ext}(X,t)$ is the external force acting on the particle. $F_{\text{int}}(X,t)$ is the internal force acting on the particle, and the particle's motion process is Figure 5.

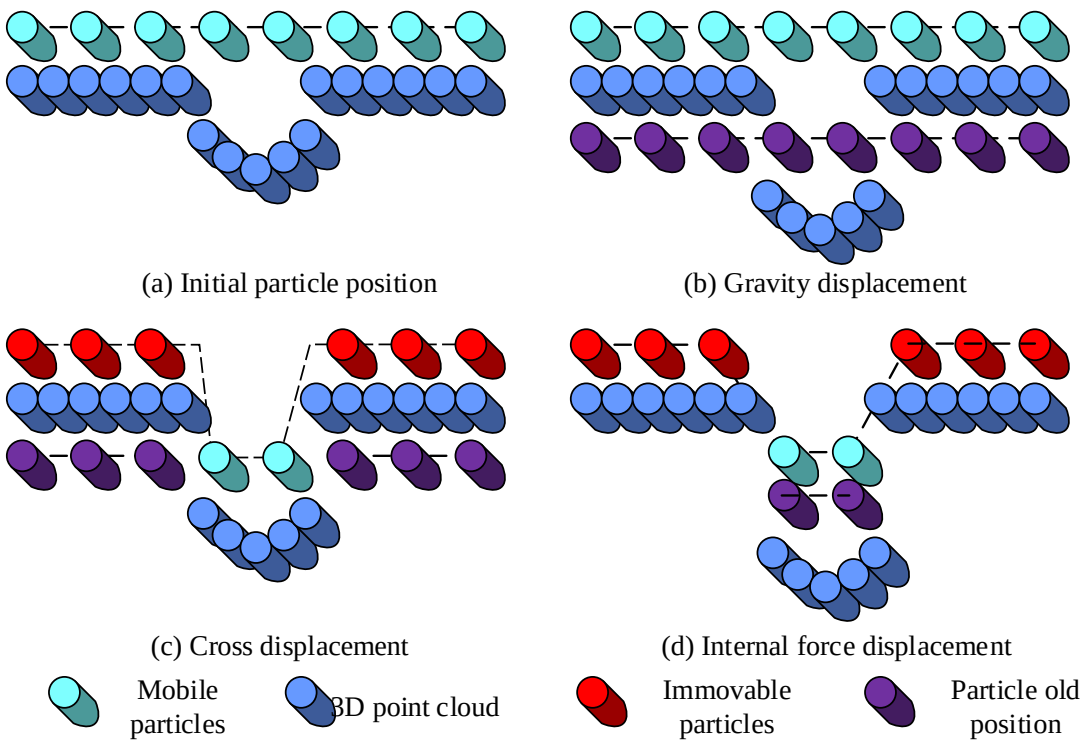

Figure 5: Particle displacement process

In Figure 5, 5 (a) shows the initial state of particles when FSF processes point cloud data. 5 (b) is when particles begin to move under the influence of gravity. 5 (c) is the occurrence of cross displacement of particles. 5 (d) is the internal driving force between particles that adjusts the movable particles. The implementation steps of FSF algorithm: 1. The point cloud is downsampled and denoised to reduce the number of points in the point cloud. The purpose of denoising is to remove noisy points from the point cloud. 2. To simulate the effect of fabric covering the point cloud, it is necessary to invert the point cloud. 3. The virtual fabric mesh is initialized and a virtual fabric mesh covering the point cloud is created. The density and size of the grid can be adjusted as needed. 4. The particles of the 3D point cloud and fabric mesh are projected onto a 2D horizontal plane for neighborhood search and height calculation. The adjacent points of each grid particle are identified, and the height of the lowest point is recorded. 5. For each fabric mesh particle, adjacent "point cloud" points are searched within their projected 2D area and the lowest height between these points is recorded. Simulating the gravitational fall of fabric particles, and the final position of particles under the influence of gravity is calculated based on the lowest height of adjacent point clouds and the current height of fabric particles. 6. Compared to the lowest point height, if the calculated final position height is less than or equal to the previously recorded lowest point height, the fabric particles are placed on the lowest point height and marked as immovable (i.e., already in contact with the ground). 7. The iteration of fabric simulation involves repeating steps 4 and 5, traversing all fabric particles until the maximum number of iterations is reached or all particles are marked as immovable. The ground points and non-ground points are classified. If the distance between a point cloud point and fabric mesh particles is less than the set threshold, it is classified as a ground point; Otherwise, it will be classified as non-ground points.

3.3 3D IBM framework design

A GIS platform that integrates BIM and SuperMap built on the Autodesk BIM application platform can construct a 3D IBM framework. However, there are certain differences in the data standards and geometric languages between the two. This study exports BIM data as Industry Foundation Classes (IFC) data, then converts IFC data into the CityGML data standard used in GIS, and finally integrates the unified data into the 3D IBM framework system. The conversion process is Figure 6.

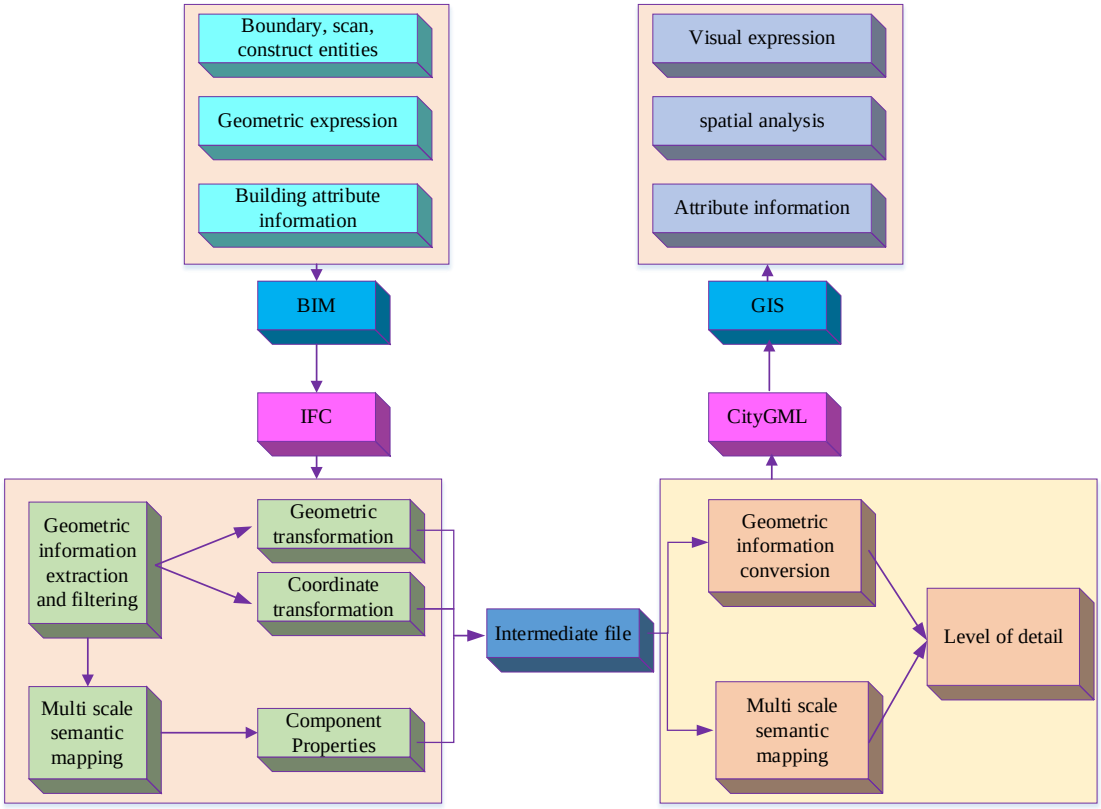

Figure 6: Conversion process between IFC data and CityGML data

In Figure 6, the conversion between IFC data and CityGML data mainly includes Geometric Information Filtering (GIF), Multi-scale Semantic Mapping (MSM), and Coordinate Transformation (CT). GIF extracts useful geometric information from IFC models to reduce redundancy and filters the types of geometric information that need to be mapped based on the CityGML standard. When integrating BIM models with GIS models, MSM is required to comply with the geometric representation requirements of CityGML. The semantic information of the IFC model is translated into CityGML format through methods such as one-to-one mapping, one-to-many mapping, and indirect mapping. To match the BIM model and oblique photography model, control points with the same name are collected, and the latitude and longitude of the BIM model insertion point are set for CT, so that the two are integrated into the same coordinate system. After integrating the BIM model and GIS model data, a 3D IBM framework is constructed, as shown in Figure 7.

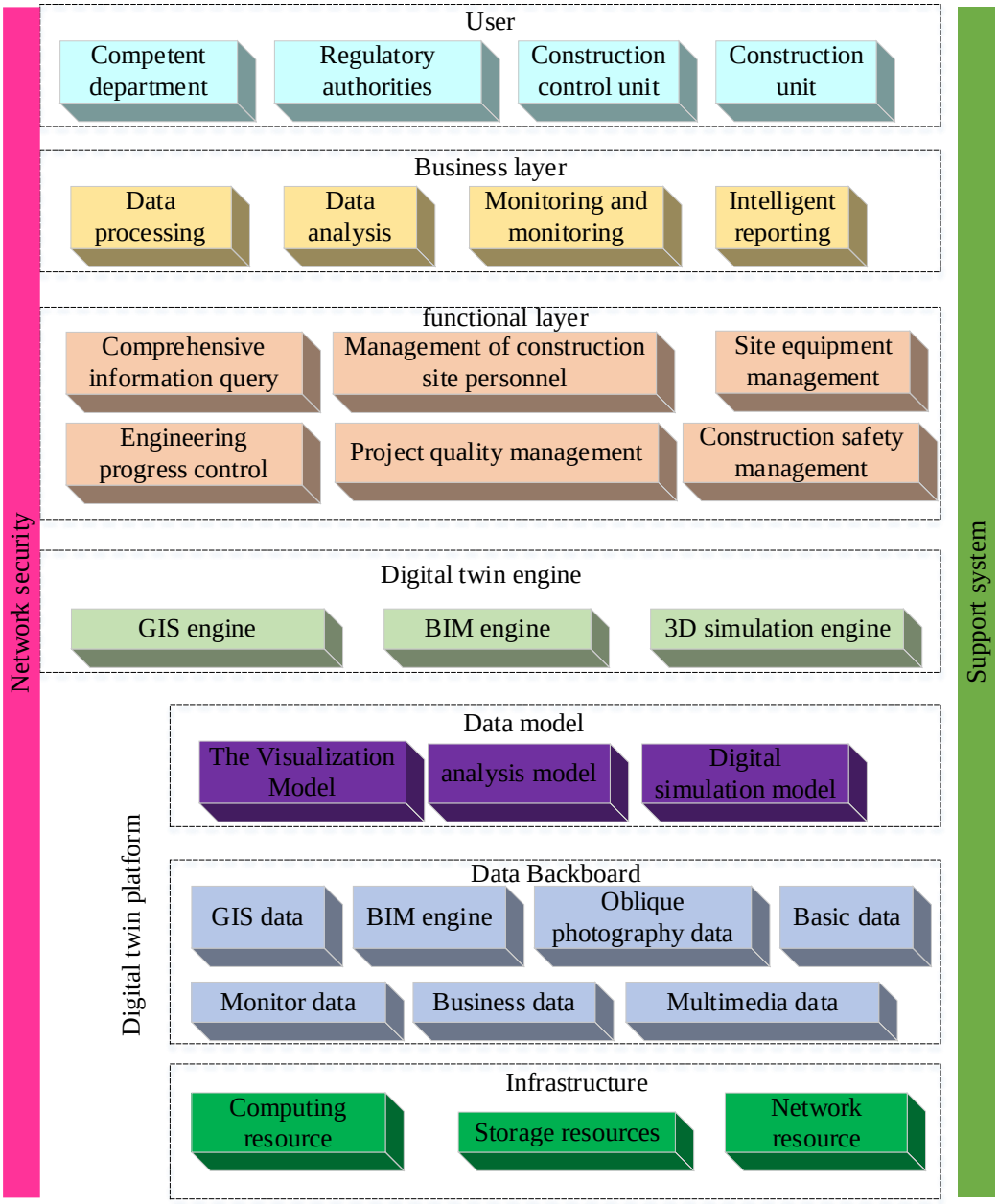

Figure 7: Design of the 3D IBM framework

In Figure 7, the 3D IBM framework mainly includes the user layer, business layer, and functional layer, which can be used for specific 3D IBM, data-driven management, and engineering application management.

4 Performance and application analysis of 3D IBM framework system

This chapter mainly constructs the environment for system development and operation, and then gradually analyzes the lightweight effect of 3D model data, the ground extraction effect of oblique photography point cloud, and the rendering effect of the system's 3D model.

4.1 Lightweight analysis of 3D model data in the system

To analyze the effectiveness of the constructed system performance, the development environment of the system is set up as displayed in Table 2.

Table 2: System development operating environment

Project	Parameter
operating system	Windows 10
Operating system	Visual Studio 2012, SuperMap Objects.Net
Database	SQL Server 2012
CPU	Core i7, dominant frequency 4.00 GHz
Memory	4GB
Hard disk	50G system, 100GB storage disk
Graphics card	4G independent graphics card with graphics card driver

Firstly, it is necessary to verify the effectiveness of the research model's lightweighting. The optimized QEM model is compressed on 7 different 3D models, and compared with the traditional QEM model, Liaf-net network model in Reference [17], and lightweight CNN model in Reference [18]. The results are shown in Figure 8.

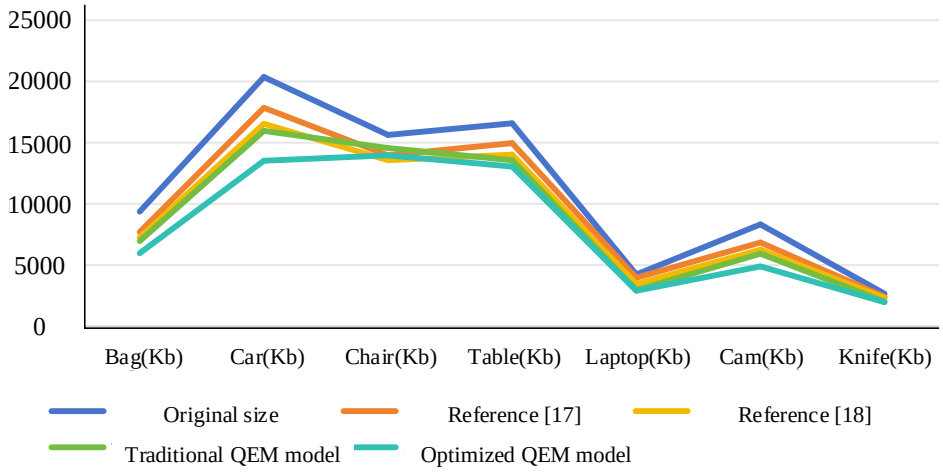

Figure 8: Comparison of the effects of different lightweight methods

In Figure 8, the optimized QEM model used in this study can effectively compress the data of the 3D model. Taking the "Car" 3D model data as an example, the original data volume is 20365Kb. After optimizing the lightweight processing of the QEM model, the data volume became 13521 and the compression rate is 66.4%. The compression rates of traditional QEM models, Liaf-net models, and lightweight CNN models are 78.3%, 81.2%, and 87.6%, respectively. This indicates that the research method can effectively perform lightweight processing on 3D data. The validity of the test results using t-square test is shown in Table 3.

Table 3: T-squared test of compression results for different models

model	Mean compression rate (%	Standard deviation of compression rate (%)	Number of observations	*t-statistic*	*P*-value
Reference [17]	81.2%	0.11	7	3.265	<0.05
Reference [18]	87.6%	0.12	7	4.623	<0.05
Traditional QEM model	78.3%	0.13	7	3.651	<0.05
Optimized QEM model	66.4%	0.01	7	1.265	<0.05

According to Table 3, the *P*-values of each test result are all less than 0.05, indicating that the results are statistically significant. To further verify the simplification effect of the research method, an optimized QEM model and a traditional QEM model are selected to simplify the 3D model of the top structure of a smart building. The simplification rates are selected as 40%, 60%, and 80%, respectively. The simplification effect is Figure 9.

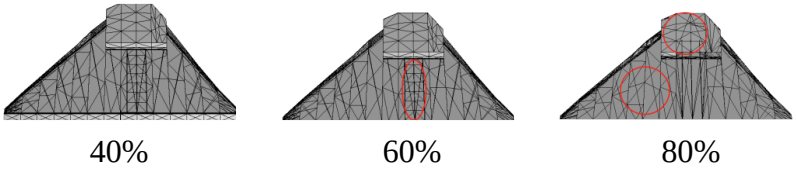

(a) Traditional QEM model

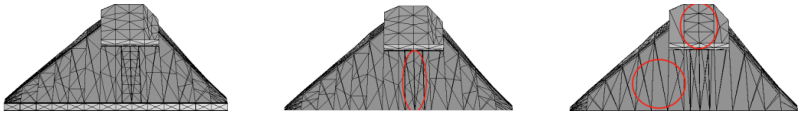

(b) Optimized QEM model

Figure 9: Simplified top model of intelligent building using different methods

In Figure 9, the optimized QEM algorithm shows similar processing results to traditional QEM algorithms when faced with a simplification rate of 40%, without any issues such as loss of model features and deformation. However, when the simplification rate reaches 60%, the improved algorithm simplifies more in flat areas compared to traditional algorithms, but retains more patches in areas with rich detailed features. When the simplification rate reaches 80%, the improved algorithm performs better in detail preservation and model deformation compared to traditional algorithms. According to data statistics, when the simplification rate is 80%, the number of patches in the 3D model decreases from 1,263,651 to 116,621, and the number of vertices decreases from 917,345 to 61,634. Moreover, the improved algorithm reduces the deformation phenomenon of the model in the grid beams and concrete panels, and avoids the loss of most patches and the occurrence of voids.

4.2 Analysis of the ground extraction effect of oblique photography "point cloud" in the system

To verify the extraction effect of oblique photography point cloud ground in the system, this study takes the construction site of a smart building project in a city as the research object. This site includes typical terrain types such as construction equipment, temporary buildings, and building materials, as well as flat, gentle, and steep slopes. According to the research method, 658 images of the area are sampled using drones, and the densely matched point cloud is Figure 10.

Figure 10: Matching point cloud data for construction site of a certain intelligent building project

To divide the research area into a 3D grid with a spacing of 50m, and set the overlapping area length to 1/15 of the 3D grid. Multiple iterative experiments are conducted on the FSF parameters to obtain the optimal parameter library. Using FSF to filter the point cloud of the target area, the filtering result of the target area is obtained, as shown in Figure 11.

Artificial Visual Interpretation of "Point Clouds"

(a) Conventional algorithm (flat) filtering results

(b) Conventional algorithm (gentle slope) filtering results

(c) Conventional algorithm (steep slope) filtering results

(d) Fabric simulation filtering algorithm

Figure 11: Comparison test results of target area filtering

As shown in Figure 11, (a), (b), (c), and (d) respectively show the extraction effects of conventional plane algorithm, conventional gentle slope algorithm, conventional steep slope algorithm, and FSF algorithm on the ground images of four regions, A, B, C, and D. In Figure 11, in the area with higher terrain (A), all four methods perform well. In the lower terrain area (B), the conventional flat parameter method and the FSF algorithm used in the study performs the best, as the conventional flat parameter method can effectively remove non-ground points on the flat ground. The FSF algorithm divides regions into flat terrain and other terrains through classification, effectively responding to terrain changes. In the steep slope area (C), the conventional steep slope parameter method performs the best, while the FSF algorithm is similar to the gentle slope parameter method, retaining the terrain but with slightly inferior results. In areas with more trees (D), the FSF algorithm uses regional grid division and inverted point cloud fitting simulation, which is slightly inferior to the conventional flat parameter method, but there are still some shorter terrains preserved. Overall, the FSF algorithm used can effectively separate ground points and non-ground points, and its effect is closest to that of manually interpreting and classifying ground point clouds. The detection accuracy results of different detection methods for the target area are shown in Table 4.

Table 4: Comparison of detection accuracy of different detection methods for target areas

Region	Method	Precision	Recall	F1 Score
A	FSF algorithm	0.92	0.93	0.93
	Conventional flat parameter method	0.90	0.92	0.92
B	FSF algorithm	0.92	0.92	0.92
	Conventional flat parameter method	0.93	0.94	0.94
C	FSF algorithm	0.90	0.90	0.90
	Conventional flat parameter method	0.93	0.94	0.94
D	FSF algorithm	0.88	0.86	0.87
	Conventional flat parameter method	0.91	0.92	0.92

According to Table 4, the FSF algorithm and conventional flat parameter method have high detection accuracy for the target area, with an F1-value almost above 0.9. To more accurately describe the differences between the research method and conventional methods, quantitative analysis is used to compare the filtering results of the four methods, as shown in Figure 12.

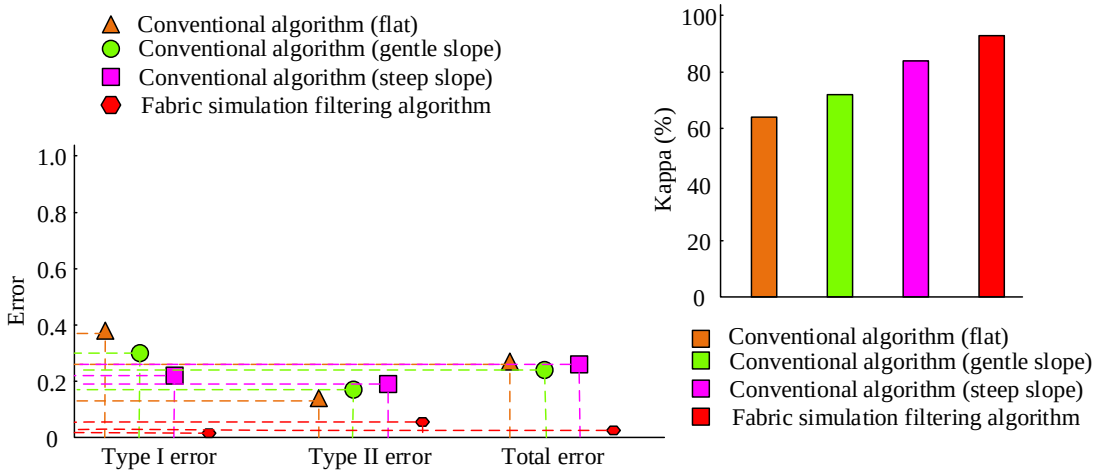

(a) Error comparison of four methods (b) Kappa comparison of four methods

Figure 12: Evaluation indicators for comparative filtering experiments in the study area

In Figure 12, the Type I and II errors and total errors of the FSF used are significantly smaller than the other three methods, with values of approximately 1.12%, 3.12%, and 2.13%, respectively. Moreover, the Kappa coefficient of this method is approximately 94.32%, indicating strong consistency in filtering performance and the ability to more accurately extract the ground "point cloud" of intelligent buildings.

4.3 Analysis of application effectiveness of 3DIBM framework system

The main appearance of a smart building is rendered using the constructed framework system, and the test results are shown in Figure 13.

The rendering effect at a distance of 20 meters | The rendering effect at a distance of 10 meters | The rendering effect at a distance of 1 meter

Figure 13: The rendering effect of the system at different distances

In Figure 13, the system can render 3D models of smart buildings at different distances, and the rendering effect can become more and more refined as the distance gets closer. At the same time, there is no lag phenomenon when the system performs rotation, scaling, and other operations during the model modeling process. Subsequently, the rendering time of the system for 3D models such as the overall appearance of intelligent buildings, intelligent system equipment, and pipelines is tested. A 3D construction system for buildings based on multi-view image sequences and a 3D reconstruction system for single tower buildings based on oblique photography technology are used as a comparison. The test results are shown in Figure 14.

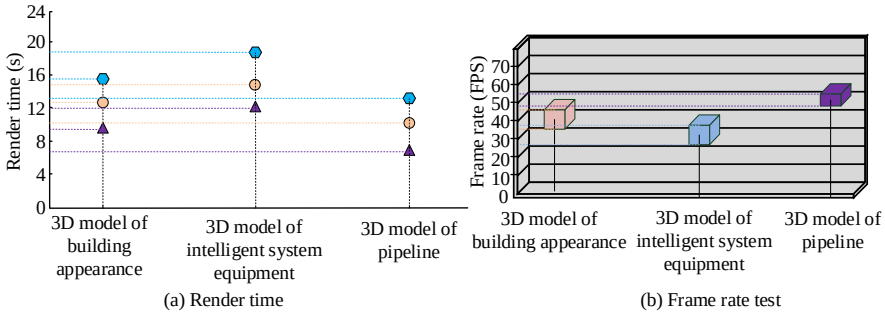

(a) Render time (b) Frame rate test

Figure 14: Comparison of 3D model rendering time and frame rate testing for different systems

In Figure 14 (a), the rendering time of the constructed system for the overall appearance of the intelligent building, intelligent system equipment, and 3D models of pipelines is 9.1s, 12.0s, and 7.2s, respectively, and the rendering time is less than the other two systems. Next, the frame rate of the system is tested when constructing 3D models of the overall appearance of the intelligent building, intelligent system equipment, and pipelines. The results are shown in Figure 14 (b). The frame rates for the three 3D models constructed by the research system are 35.2-46.2FPS, 27.6-38.1FPS, and 48.2-53.1FPS, respectively. According to the data, the comfort zone of the human eye is 24 FPS, and the frame rate used in constructing the model of the research system meets the requirements of the human eye's comfort zone. In addition, after testing, the system can also be compatible with various browsers including Chrome, 360 browser, IE10 browser, and can smoothly complete all functions of the 3D intelligent building framework management system in these browsers.

5 Discussion and conclusion

Integrating BIM and GIS data can quickly achieve 3D IBM design. The data fusion between BIM and GIS is mainly achieved through the extension of data standards and the conversion of data formats. IFC and CityGML are the main data standards in the fields of BIM and GIS, and researchers are attempting to address data integration issues by developing new standards or unifying building models. To this end, a BIM was built using the Autodesk BIM application platform, a GIS 3D model was built using the SuperMap series software, and a 3D IBM framework system was constructed by fusing BIM data information and GIS data information using a data transformation-based method. By integrating two technologies, a 3D model containing rich geographic and architectural information could be constructed, providing comprehensive and accurate information support for the planning, design, construction, operation and maintenance stages of building projects. Among them, the optimized QEM model used in the study could easily achieve lightweighting of BIM data, and had better data compression performance compared to traditional QEM models, Liafnet neural network models, and lightweight CNN network models. This is because the optimized QEM model can more accurately retain important features of the model, while removing redundant vertices and patches, thereby achieving a significant reduction in data volume. When the simplification rate reached 80%, the research method was more meticulous in preserving details and processing deformation in model construction. The FSF algorithm used in the study could effectively separate ground points and non-ground points, and its processing effect was closest to that of manually interpreting and classifying ground "point clouds". Compared with other methods, the FSF algorithm could adapt to different terrain and geomorphic features, including plains, mountains, steep slopes, etc., reducing misjudgment and missed judgments. Moreover, the algorithm had a fast execution speed and could process a large amount of point cloud data in a short time. The system constructed in the study could render 3D models at different distances, with rendering times of 9.1s, 12.0s, 7.2s for the overall appearance of intelligent buildings, intelligent system equipment, and pipelines, and other 3D models. The frame rates during rendering were 35.2-46.2FPS, 27.6-38.1FPS, 48.2-53.1FPS. The fast-rendering time and high frame rate made it possible for the system to support real-time interaction. Based on the above data, it can be concluded that the research model can effectively achieve complementary integration of geographic environment spatial data and intelligent BIMs, providing a more intuitive visual engineering management mode for 3D intelligent building projects. However, the management module constructed through research has a relatively single function, and the functionality of the management design framework will be further enriched and improved in the later stage.

Funding

The research is supported by The Visiting Scholar and Visiting Engineer Project (Theory) of Zhejiang Province University "Application Research of BIM Technology Based on Whole Life Cycle in Hangzhou National Version Library" (No. FG2022042).

References

[1] Himeur Y, Elnour M, Fadli F, Meskin N, Petri I, Rezgui Y. AI-big data analytics for building automation and management systems: a survey, actual challenges and future perspectives. Artificial Intelligence Review, 2023, 56(6): 4929-5021. https://doi.org/10.1007/s10462-022-10286-2

[2] Ross P, Maynard K. Towards a 4th industrial revolution. Intelligent Buildings International, 2021,

13(3): 159-161. https://doi.org/10.1080/17508975.2021.1873625

[3] Sun Z, Anbarasan M, Praveen Kumar D. Design of online intelligent English teaching platform based on artificial intelligence techniques. Computational Intelligence, 2021, 37(3): 1166-1180. https://doi.org/10.1111/coin.12351

[4] Deng Z, Chen Y, Yang J, Chen Z. Archetype identification and urban building energy modeling for city-scale buildings based on GIS datasets. Building Simulation. Beijing: Tsinghua University Press, 2022, 15(9): 1547-1559. https://doi.org/10.1007/s12273-021-0878-4

[5] Xiao Y, Bhola J. Design and optimization of prefabricated building system based on BIM technology. International Journal of System Assurance Engineering and Management, 2022, 13(l1): 111-120. https://doi.org/10.1007/s13198-021-01288-4

[6] Yu L, Qin S, Zhang M, Shen C, Jiang T, Guan X. A review of deep reinforcement learning for smart building energy management. IEEE Internet of Things Journal, 2021, 8(15): 12046-12063. https://doi.org/10.48550/arXiv.2008.05074

[7] Edirisinghe R, Woo J. BIM-based performance monitoring for smart building management. Facilities, 2021, 39(1/2): 19-35. https://doi.org/10.1108/F-11-2019-0120

[8] Pan Y, Zhang L. Integrating BIM and AI for smart construction management: current status and future directions. Archives of Computational Methods in Engineering, 2023, 30(2): 1081-1110. https://doi.org/10.1007/s11831-022-09830-8

[9] Abd A M, Hameed A H, Nsaif B M. Documentation of construction project using integration of BIM and GIS technique. Asian Journal of Civil Engineering, 2020, 21(7): 1249-1257. https://doi.org/10.1007/s42107-020-00273-9

[10] Asgari Siahboomy M, Sarvari H, Chan D W M, Nassereddine H, Chen Z. A multi-criteria optimization study for locating industrial warehouses with the integration of BIM and GIS data. Architectural Engineering and Design Management, 2021, 17(5-6): 478-495. https://doi.org/10.1080/17452007.2021.1881880

[11] Zhu J, Tan Y, Wang X. BIM/GIS integration for web GIS-based bridge management. Annals of GIS, 2021, 27(1): 99-109. https://doi.org/10.1080/19475683.2020.1743355

[12] AlSaggaf A, Jrade A. ArcSPAT: an integrated building information modeling (BIM) and geographic information system (GIS) model for site layout planning. International Journal of Construction Management, 2023, 23(3): 505-527. https://doi.org/10.1080/15623599.2021.1894071

[13] Dinis F M, Poças Martins J, Guimarães A S, Rangel B. BIM and semantic enrichment methods and applications: a review of recent developments. Archives of Computational Methods in Engineering, 2022, 29(2): 879-895. https://doi.org/10.1007/s11831-021-09595-6

[14] Mahmood T, Ali Z. Prioritized muirhead mean aggregation operators under the complex single-valued neutrosophic settings and their application in multi-attribute decision-making. Journal of Computational and Cognitive Engineering, 2022, 1(2): 56-73. https://doi.org/10.47852/bonviewJCCE2022010104

[15] Debnath S. Fuzzy quadripartitioned neutrosophic soft matrix theory and its decision-making approach. Journal of Computational and Cognitive Engineering, 2022, 1(2): 88-93. https://doi.org/10.47852/bonviewJCCE19522514205514

[16] Qin W, Wen H, Li F. Fabric defect detection algorithm based on residual energy distribution and Gabor feature fusion. The Visual Computer, 2023, 39(11): 5971-5985. https://doi.org/10.1007/s00371-022-02706-9

[17] Wu Z, Zhang H, Lin Y, Li G, Wang M, Tang Y. Liaf-net: Leaky integrate and analog fire network for lightweight and efficient spatiotemporal information processing. IEEE Transactions on Neural Networks and Learning Systems, 2021, 33(11): 6249-6262. https://doi.org/10.48550/arXiv.2011.06176

[18] Tsai C Y, Su Y K. MobileNet-JDE: a lightweight multi-object tracking model for embedded systems. Multimedia Tools and Applications, 2022, 81(7): 9915-9937. https://doi.org/10.1007/s11042-022-12095-9